ADVANCED ENGINEERING MATERIALS
www.aem-journal.com

Wire-Laser-Directed Energy Deposition of Ti-6Al-4V Alloy Under Vacuum: Effect of Substrate Preheating on the Refinement of Prior-β Grain Structure

Haneen Daoud, Agata Kulig, Kim Schmidt, Johannes Weiser, Maximilian Fichtl, Andrey Prihodovsky, and Uwe Glatzel*

The effect of stress relieving and substrate preheating on the grain refinement of additively manufactured Ti-6Al-4V at room and elevated temperatures is investigated. Specimens are produced using wire-based directed energy deposition under vacuum conditions. The microstructure is characterized by scanning electron microscopy (SEM), electron backscatter diffraction (EBSD), and X-ray diffraction (XRD). Tensile tests are conducted at room temperature and at 700 °C. The as-deposited specimens exhibit a heterogeneous microstructure consisting of fine acicular α′-martensite and fine Widmanstätten structures. Substrate preheating at 600 °C enables a complete transition from a columnar grain structure in the as-deposited condition to a refined prior-β grain structure. The as-substrate-heated specimens show the highest tensile strength of 1010 MPa with 3% elongation at room temperature and 600 MPa with 15% elongation at 700 °C.

1. Introduction

α + β titanium alloys with high levels of β-stabilizers such as Ti-6Al-4V are among the most widely researched titanium alloys in the field of additive manufacturing (AM).[1–3] They have already been successfully applied in printed form and are particularly prominent in the aerospace and medical industries due to their excellent biocompatibility, low density, and high specific strength.[4–11]

The microstructure of Ti-6Al-4V is highly sensitive to solidification conditions and the thermal history of the manufacturing process.[2,3,12,13] At room temperature, the alloy typically consists of a hexagonal close-packed (HCP) α-phase and a body-centered cubic (BCC) β-phase.[14,15] In AM, the β-phase transforms back to the primary α-phase under low cooling rates, or to a martensitic α′-phase under high cooling rates. The volume fraction and morphology of the α-phase are strongly influenced by the cooling rate.[2,12,13] The grain structure of Ti-6Al-4V is typically characterized by planar growth across all AM processes, including laser powder bed fusion (PBF-LB/M) and electron beam melting (PBF-EB/M), despite the high solidification rates involved.[3,12] Bermingham et al. investigated the role of solute elements in grain-refining mechanisms in Ti-6Al-4V and attributed this phenomenon to the high partition coefficients of aluminum and vanadium in titanium, which are close to one.[16] A. A. Antonysamy et al. proposed an additional explanation for the formation of planar grains, suggesting that the narrow solidification range of Ti-6A-l4V limits the degree of constitutional supercooling, thereby reducing the nucleation of equiaxed grains.[17] The influence of alloying elements such as Ni, Co, and Cu has been investigated to promote the columnar-to-equiaxed grain transition in titanium alloys.[18–20]

The mechanical properties of Ti-6Al-4V alloy are strongly influenced by its microstructure, which is determined by manufacturing process and can be tailored through appropriate heat treatment.[21–24] PBF-LB/M leads to the formation of a martensitic α′-phase (acicular) at high cooling rates. This results in a high tensile strength of around 1260 MPa at room temperature and an elongation of ≈7%.[25] Elongation can be improved to over 10% by applying different heat treatments or hot isostatic pressing (HIP) to the as-built specimens. However, the tensile strength

H. Daoud, A. Kulig, K. Schmidt, U. Glatzel
Metals Division
Neue Materialien Bayreuth GmbH
Gottlieb-Keim-Str. 60, 95448 Bayreuth, Germany
E-mail: Haneen.Daoud@nmbgmbh.de

The ORCID identification number(s) for the author(s) of this article can be found under https://doi.org/10.1002/adem.202502223.

DOI: 10.1002/adem.202502223

K. Schmidt
Tatajuba Solutions GmbH
Heßstr. 89, 80797 München, Germany

J. Weiser
Evobeam GmbH
Am Hofgut 5, 55268 Nieder-Olm, Germany

M. Fichtl, A. Prihodovsky
Technologie Campus Parsberg-Lupburg
Am Campus 1, 92331 Parsberg, Germany

U. Glatzel
Metals and Alloys
University of Bayreuth
Prof.-Rüdiger-Bormann-Str. 1, 95447 Bayreuth, Germany

decreases to a range of 840–1000 MPa due to the formation of a lamellar mixture of α and β upon cooling.[22,25–28] A mixture of fine α- and β-phases solidified during the PBF-EB/M processing of Ti-6Al-4V specimens due to the greater penetration depth, which led to lower cooling rates compared to PBF-LB/M.[29,30] Subsequently, a lower tensile strength of ≈930–980 MPa was observed, accompanied by higher elongation exceeding 9.5%, attributed to the presence of lamellar α-phase.[29] Higher applied laser power, combined with slow cooling rates resulting from multiple repeated thermal cycles during powder-based directed energy deposition Laser beam Direct Energy Deposition for metal additive manufacturing (DED-LB/M), enhances the stabilization of a heterogeneous microstructure. This depends not only on the applied process parameters but also on the distance from the cooled substrate. Colonies of α-Widmanstätten morphology, including basket-weave structures, along with large prior-β grains, are the main characteristic features of the as-deposited microstructure in Ti-6Al-4V specimens.[31–34] The as-deposited Ti-6Al-4V specimens exhibit a high tensile strength of 1000–1100 MPa and an elongation exceeding 10%.[35]

Wire-based AM has been increasingly used in recent years for the rapid fabrication of Ti-alloys for large-scale lightweight components.[36–40] Wire-arc directed energy deposition (DED) is the most extensively researched technique for processing different types of titanium alloys, including both α + β and β-phase alloys.[36–41] G. Zhang et al. reported a tensile strength of 953 MPa with a 6% elongation at room temperature for as-deposited Ti-6Al-4V specimens fabricated using wire-arc DED.[41] However, the resulting large melt pools and high thermal gradients in the as-deposited specimens promote microstructural coarsening and anisotropic mechanical properties.[36–41] Similar microstructural behavior has also been observed in as-deposited Ti-6Al-4V specimens fabricated via wire-laser DED.[42] P. Akerfeldt et al. produced wire-laser DED Ti-6Al-4V specimens with tensile strengths ranging from 850 to 950 MPa, depending on the printing direction, and elongations between 10% and 18%.[42] Wire-laser DED is still rarely researched for Ti-alloys; however, compared to the wire-arc DED process, it produces shorter melt pools, which could help stabilize the desired microstructure. Nevertheless, oxidation during wire-based DED remains an issue that needs to be resolved. The presence of a heterogeneous microstructure, combined with significant thermal gradients and resulting anisotropic mechanical properties, remains the primary obstacle to the broader application of wire-based DED for fabricating large Ti-6Al-4V components. These challenges constitute the primary motivation for this study.

In this work, a wire-based DED process operating under vacuum (10^{-3} mbar) is used to deposit Ti-6Al-4V components. The primary focus of the study is to investigate the influence of substrate preheating temperature on reducing thermal gradients and enhancing the homogeneity of the resulting microstructure. In addition, the evolution of oxygen content during repeated thermal cycles will be examined. Microstructural characterization and tensile testing at both room and elevated temperatures will be carried out on the as-deposited materials as well as after stress relief heat treatment.

Table 1. Chemical composition of Ti-6Al-4V alloy in weight percentage.

Al	V	O	Fe	H	C	N	Ti
6.2	4.0	<0.2	<0.3	<0.0015	<0.08	<0.05	Rest

2. Experimental Section

The wire used in this study was a titanium alloy, Ti-6Al-4V (Grade 5, E. Reim GmbH, Germany), with a diameter of 1.0 mm. The chemical composition is given in **Table 1**. Substrates made from the same titanium alloy were used, with dimensions of 180 × 90 mm and a thickness of 15 mm. Prior to printing, the substrate surface was sandblasted using 99.8% Al_2O_3 (SMG 100, MHG Strahlanlagen GmbH, Germany).

The wire-based laser direct energy deposition (DED-LB/M) system under vacuum used was developed by Evobeam GmbH (**Figure 1**a,b). The DED-LB/Ti-6Al-4V process was conducted in a vacuum chamber maintained at 10^{-3} mbar, combined with an argon shielding mechanism at a flow rate of 4 L min^{-1}. Two external heat sources were employed: an IPG Photonics YLR laser system with a 2 kW laser power and a preheating system integrated into the wire feeder. The wire preheating system operated at a maximum power of 220 A. The wire feeder nozzle was positioned at a 30° angle relative to the

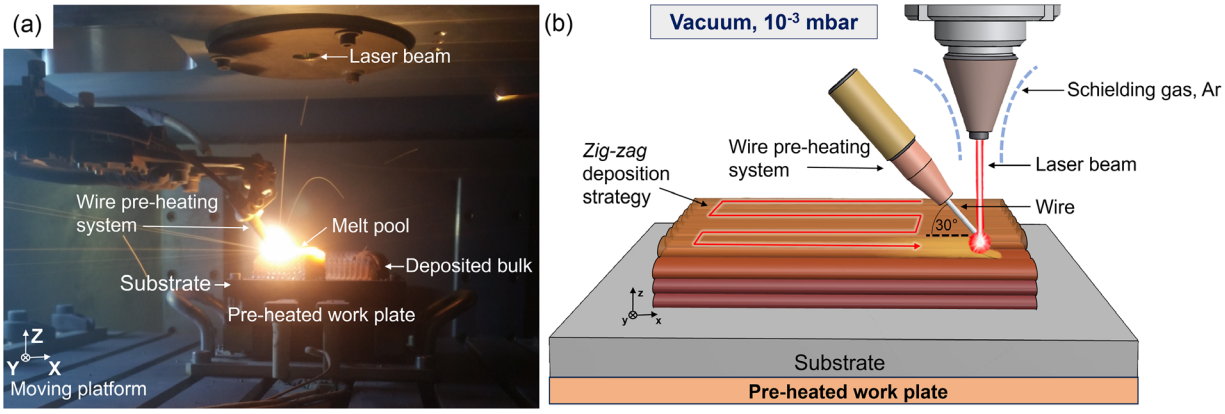

Figure 1. a) In situ photograph capturing the DED-LB/M process in operation, developed by Evobeam GmbH. b) Schematic illustration of the DED-LB/M process, which uses a preheated substrate and wire preheating as secondary external heat sources.

Table 2. Applied process parameters for printing of as-deposited blocks.

Parameter	30% of the initial printed layers	Rest of the printed specimen
Laser power [kW]	1600	100
Wire heating [A]	132	110
Wire feed speed [mm min^{-1}]	1800	1800
Table speed [mm s^{-1}]	650	650
Wobbler Radius (W_R) [mm]	0.8	1.0

Table 3. Summarizes the different test conditions of the printed specimens along with their abbreviations used in this study.

As-deposited-bulk	Without substrate heating, without any stress-relieving
As-deposited-Stress-relieved (SR)	Without substrate heating, stress-relieved at 800 °C/4 h
As-substate-heated	With 800 °C substrate heating, without any stress-relieving
As-substate-heated-SR	With 800 °C substrate heating, stress-relieved at 800 °C/4 h

substrate surface. The movement of the work table in X and Y axes (horizontal plane) was controlled by a CNC table (SINUMERIC D5000 system, SIEMENS, Germany). The applied process parameters, including laser power, wire feed speed, table speed, energy required for wire heating, and wobbler radius, are summarized in **Table 2** (only the optimized parameters are shown). To investigate the influence of substrate heating, the substrate was inductively preheated to a temperature of 800 °C for some printing tests. The printed specimens have the dimensions of 55 × 4 × 45 mm (**Figure 2**a–c). To minimize pore formation, the deposition path was rotated by 90° for each subsequent layer (zig–zag deposition strategy, Figure 1).

The process parameters were not constant throughout the entire manufacturing process. Initially, high laser power and significant wire heating were necessary to ensure proper wire melting. However, after ≈30% of the specimen volume was built, both laser power and wire heating were reduced to prevent excessive melting and minimize layer overlap (Figure 2a,b).

The as-deposited specimens were stress-relieved at 800 °C for 4 h under an argon atmosphere in a furnace (HK-315, Linn High Therm GmbH, Germany), following DIN 65 084. Cooling was performed first in the furnace, then in air. For microstructural analysis, specimens were cut from the as-deposited bulk in two orientations: longitudinal (X–Y) and cross-section (Z), as shown in Figure 2c.

Cross-sections of all the tested specimens were grounded and polished and etched with the Kroll's etching reagent for microstructural investigations using optical (Axioskop, Carl Zeiss AG, Germany) and electron microscopies. The microstructure and chemical composition were characterized using a scanning electron microscope (SEM, Zeiss EVO MA15, Germany) equipped with an energy-dispersive X-ray spectrometer (EDX). For electron backscatter diffraction (EBSD) analysis, the specimens were further polished for 8 h using a 0.08 µm OP-U colloidal silica suspension on a VibroMet 2 vibratory polishing machine (Buehler, Esslingen, Germany). The SEM used for the EBSD analyses was a TESCAN MIRA4 GMU, equipped with an EDAX Velocity Pro EBSD camera. Oxygen and nitrogen content were determined based on the carrier gas hot extraction technique (EMGA-Emia, HORIBA Yobin Yvon, Japan). Phase identification was performed by X-ray diffraction (XRD, Bruker D8 advance diffractometer, Germany).

Tensile tests were conducted on as-deposited and as-substate-heated specimens at room temperature (RT) and at 700 °C using a tensile testing device (DDS-3, Kammrath & Weiss GmbH, Germany) at a strain rate of ≈1.3×10^{-3}s^{-1}. Flat tensile specimens (Figure 2d) with a total length of 49 mm, a gauge length of 15 mm, and a thickness of 1 mm were prepared. As shown in Figure 2c, the test samples were cut from the longitudinal section (X-Y) of Area 2, perpendicular to the deposition direction (Z).

The different test conditions of the printed specimens and their corresponding abbreviations are listed in **Table 3**.

3. Results

3.1. Microstructure of Printed DED-LB/Ti-6Al-4V Specimens

3.1.1. As-Deposited Specimens

The as-deposited specimens, both with and without stress-relieving, as shown in **Figure 3**a,b, exhibit irregular equiaxed

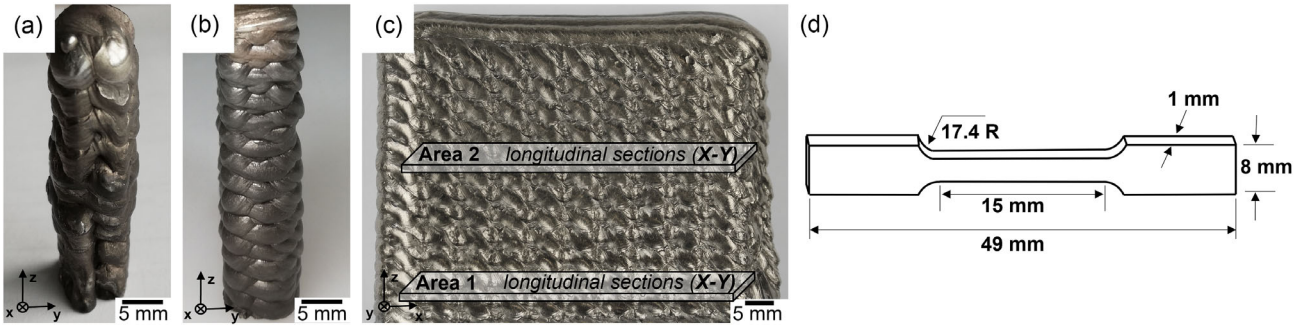

Figure 2. Images illustrating the impact of DED-LB process parameters on as-deposited-bulk Ti-6Al-4V specimens under two conditions: a) with constant process parameters; b) with reduced laser power and wire heating after ≈30% of the specimen's volume was deposited; and c) front view of the as-deposited block, indicating the region selected for microstructural analysis, and d) dimensions of the tensile test specimens.

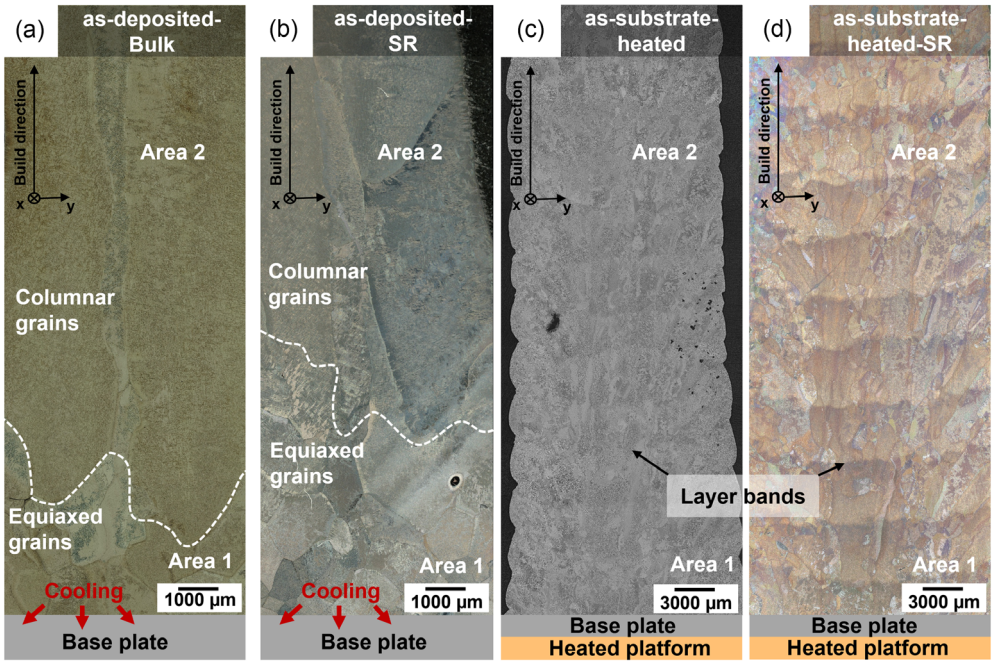

Figure 3. Optical micrographs of the printed specimens: a) as-deposited-bulk, b) as-deposited-SR, c) as-substrate-heated, and d) as-substrate-heated-SR.

grain formation with sizes approximately between 1 and 1.5 mm in the lower region near the substrate. This region extends about 5 mm in the as-deposited-bulk specimens and ≈10 mm in the as-deposited-Stress-relieved (SR) specimens. In the middle and upper regions, large prior-β columnar grains aligned parallel to the build direction are stabilized, with lengths exceeding 10 mm and widths ranging from 1 to 3 mm in both tested as-deposited specimens.

The SEM micrograph of the lower region (Area 1) of the as-deposited-bulk specimen (**Figure 4**b) reveals very fine acicular α′-martensite structures. In contrast, a coarser α + β phase mixture in the form of a fine basket weave (Widmanstätten structure) is observed in Area 2 (Figure 4a). Grain boundaries (α_{GB}) in both areas are visible in Figure 4a,b. In Area 2, the primary alpha (α) phase is oriented perpendicularly to the α_{GB}. In the case of the as-deposited-SR specimens, both analyzed areas exhibit a coarsening of the basket weave (Widmanstätten structure) compared to the as-deposited-bulk specimens (Figure 4c,d). The thickness of the grain boundaries (α_{GB}) is noticeably greater in the upper regions than in the lower regions. The α-lamellae width in the as-deposited-bulk specimens is ≈1.0 µm, whereas in the as-deposited SR specimens, it is about 2.5 µm. EBSD images reveal the growth of large prior-β columnar grains aligned parallel to the build direction in both the as-deposited-bulk and as-deposited-SR specimens

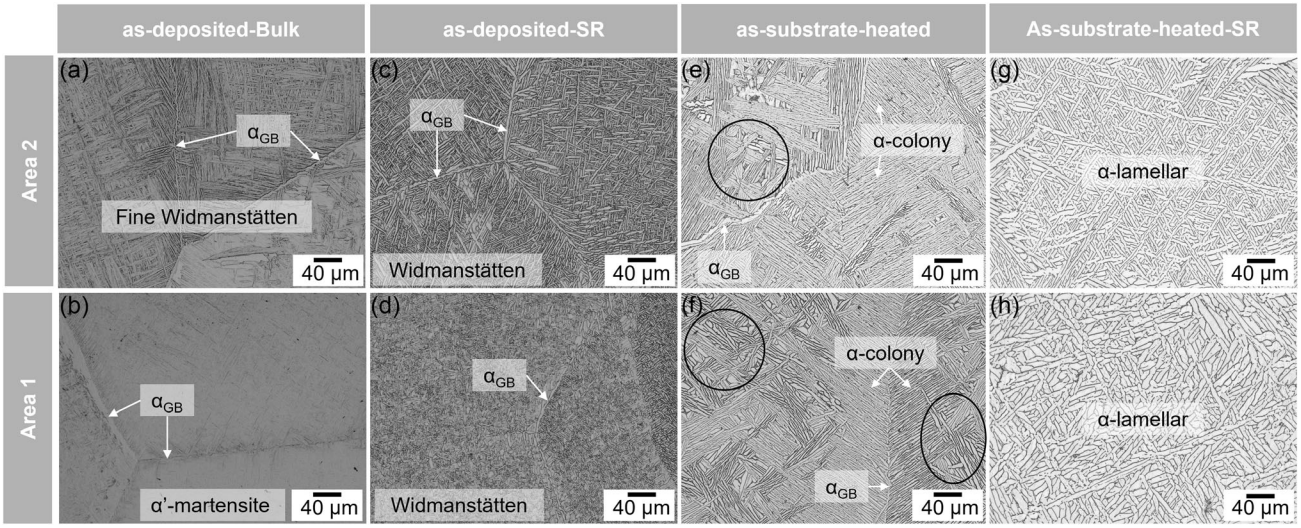

Figure 4. SEM micrographs of the specimens a,b) as-deposited-bulk, c,d) as-deposited-SR, e,f) as-substrate-heated, and g,h) as-substrate-heated-SR.

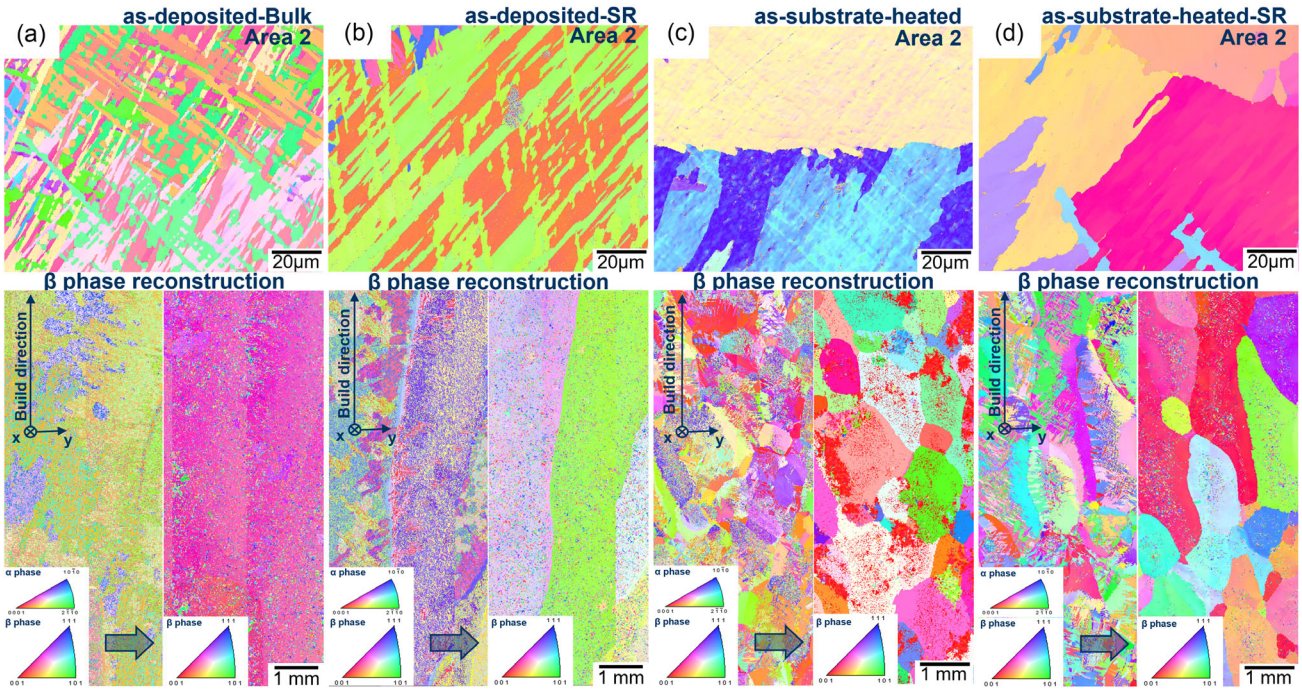

Figure 5. EBSD images and large area mapping for a) as-deposited-bulk, b) as-deposited-SR, c) as-substrate-heated, and d) as-substrate-heated-SR.

(**Figure 5**a,b). A finer Widmanstätten structure is observed in the as-deposited-bulk compared to the as-deposited-SR.

The XRD pattern of the as-deposited-bulk specimen in the lower region (Area 1) shows peaks corresponding to the α′, α, and β phases (**Figure 6**a,b). The α′ peaks are clearly visible in the enlarged section of the diffraction pattern shown in Figure 6c. In Area 2, only peaks related to the α and β phases are present. For the as-deposited-SR specimens, the XRD patterns in both areas 1 and 2 display peaks corresponding to the α and β phases, with a substantial reduction in β-phase peak intensity observed in both regions (Figure 6a,b).

3.1.2. As-Substrate-Heated Specimens

The optical images show an irregular formation of equiaxed grains in both as-substrate-heated specimens. The grain sizes range from 0.5 to 3 mm in the as-substrate-heated condition and from 1 to 5 mm in the as-substrate-heated-SR specimens (Figure 3c,d). In both cases, the layer bands are clearly visible and evenly spaced throughout the structure, with thicknesses of 3 mm and 4.5 mm in the as-substrate-heated and as-substrate-heated-SR specimens, respectively. Grain growth is continuous across the layer bands.

The lower region (area 1) of the as-substrate-heated specimens exhibits a mixture of coarse Widmanstätten structures (marked with a circle) and α-colonies. In contrast, the upper regions (area 2) show a higher concentration of α-colonies with only small areas of Widmanstätten structures (Figure 4e,f). The average α-lamellae width in the as-substrate-heated specimens is ≈2.8 μm. Very coarsened α-lamellar are observed in the as-substrate-heated-SR specimens, with an average α-lamellae width of ≈4 μm (Figure 4g,h). However, the α-plates are slightly thinner in the upper region (Area 2) compared to the lower region (Area 1).

The EBSD images show the formation of equiaxed grains with no preferred orientation in both as-substrate-heated conditions (Figure 5c,d). The XRD patterns of the as-substrate-heated-SR shows strong peaks belonging to α-phase (Figure 6a,b).

3.2. Oxygen and Nitrogen Content

Figure 7 illustrates the oxygen (O_2) and nitrogen (N_2) content, measured in parts per million (ppm), across three different processing conditions of DED-LB/Ti-6Al-4V: as-deposited-bulk, as-deposited-SR, and as-substrate-heated-SR, as well as the initially used wire (Ti-6Al-4V).

A clear increasing trend in oxygen content is observed across the processing conditions. Starting at ≈35 ± 0.8 ppm in the wire, the oxygen concentration progressively increases in the as-deposited specimens, reaching a maximum of 197 ± 31 ppm in the as-substrate-heated-SR condition. In contrast, the nitrogen content remains relatively stable across all conditions, ranging from 1.1 ± 0.8 ppm in the initial wire to a maximum of 3 ± 1.6 ppm in the as-deposited specimens.

3.3. Mechanical Properties

3.3.1. As-Deposited Specimens

The Vickers hardness (HV1) is ≈336 for the as-deposited-bulk specimen and 344 for the as-deposited-SR specimen, as shown in **Figure 8**a. The tensile strength at room temperature for the as-deposited-bulk specimen is 750 MPa, with an elongation of

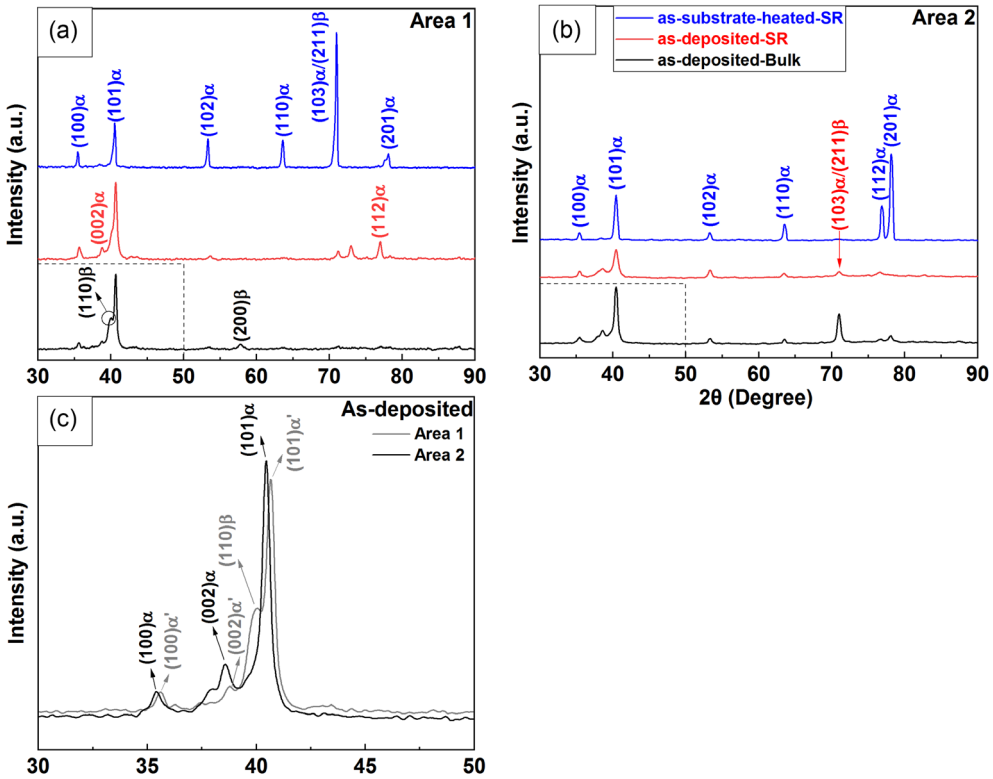

Figure 6. a,b) XRD diffraction patterns of all tested specimens in both Areas 1 and 2, and c) enlarged section of the diffraction pattern for the as-deposited-bulk specimens.

5%–6%. In contrast, the as-deposited-SR specimens exhibit a higher tensile strength of 850 MPa and with a notable improvement in ductility, reaching 10%–11% (Figure 8b).

At 700 °C, the tensile strength of the as-deposited-SR specimen is 400 MPa, with an elongation of ≈9%. No tensile testing was conducted for the as-deposited-bulk specimens due to their lower mechanical properties at room temperature.

3.3.2. As-Substrate-Heated Specimens

The average Vickers hardness is 392 for the as-substrate-heated specimens and 436 for the as-substrate-heated-SR specimens (Figure 8a). At room temperature, both the as-deposited-bulk and as-deposited-SR specimens exhibit similar tensile mechanical behavior, with a tensile strength of 1010 MPa and an elongation of 3% (Figure 8b).

At 700 °C, tensile strengths of ≈600 MPa and 500 MPa were measured for the as-substrate-heated and as-substrate-heated-SR specimens, respectively. The elongation exceeded 9% for the as-substrate-heated-SR specimens and reached around 14%–15% for the as-substrate-heated specimens (Figure 8c).

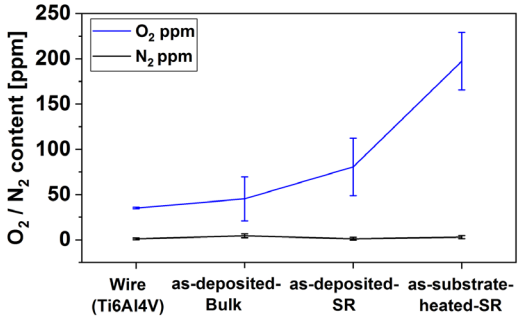

Figure 7. Measured oxygen (O_2) and nitrogen (N_2) content in the as-deposited-bulk, as-deposited-SR, and as-substrate-heated-SR specimens, compared to the initially used wire. Error bars represent the standard deviation based on a minimum of three measurements.

4. Discussion

4.1. Effect of Stress Relieving and Substrate Heating on the Microstructural Evolution of as-Deposited Specimens

The formation of planar (columnar) grains in additively manufactured specimens of the Ti-6Al-4V alloy is a common phenomenon.[3,12,16,17] The columnar grain structure results from the combined effect of the high thermal gradient during solidification and the minimal solute segregation. However, in this study, the growth of equiaxed grains near the substrate surface in both the as-deposited-bulk and as-deposited-SR specimens can be attributed to the cold substrate surface (Figure 3a,b). This condition promotes the nucleation of equiaxed grains in localized regions near the surface. Nevertheless, due to the repeated thermal cycling during the DED-LB/M process, the high thermal gradients and low cooling rates in the upper deposited layers inhibit

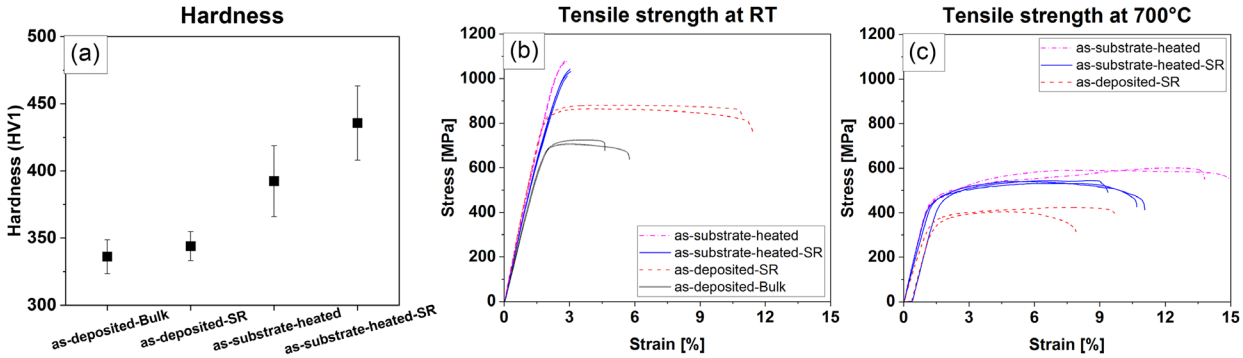

Figure 8. a) Vickers hardness (HV1) of all tested specimens with error bars representing the standard deviation based on a minimum of three measurements, and b,c) tensile stress–strain curves (b) at room temperature (RT) and (c) at 700 °C.

the nucleation of equiaxed grains across the entire printed block. The high thermal gradient in both as-deposited-bulk and as-deposited-SR specimens promotes the heterogeneous microstructure, as shown in Figure 4a–d and Figure 5a,b. The higher cooling rates in the regions near the substrate promote the formation of a fine α′-martensitic structure. In contrast, in the upper regions of the printed specimens, a fine Widmanstätten structure with α-lamellae widths below 2 μm is observed in the as-deposited-bulk specimens. The effect of high cooling rates and rapid solidification on the stabilization of very fine α′-martensitic and Widmanstätten structures has been reported previously.[2,17,43,44] Stress relieving at 800 °C for 4 h in the as-deposited specimens tends to promote the formation of a fine Widmanstätten structure in the lower regions (area 2) and a slightly coarser Widmanstätten structure with α-lamellae widths of ≈2.5 μm in the upper regions (area 1). Heat treatment below the β-transus temperature (994 °C) leads to fine α-precipitation and martensite decomposition, rather than the formation of a coarser α and β mixture.[2,23,43,44] Due to the nonuniform cooling rates within the same deposited block, the microstructural evolution pathway can be described as follows

$$\text{(as-deposited-Bulk) lower regions } L \rightarrow \beta \rightarrow \text{(fine) } \alpha' + \text{(fine) } \alpha_{GB} \quad (1)$$

$$\text{(as-deposited-Bulk) upper regions } \alpha' \rightarrow \text{(fine) } \alpha + \beta + \text{(fine) } \alpha_{GB} \quad (2)$$

$$\text{(as-deposited-SR) lower regions } \alpha' \rightarrow \text{(fine) } \alpha + \beta + \text{(fine) } \alpha_{GB} \quad (3)$$

$$\text{(as-deposited-SR) upper regions } \alpha' \rightarrow \text{(fine) } \alpha + \beta + \text{(fine) } \alpha_{GB} \quad (4)$$

Continuous substrate heating at 600 °C throughout the DED-LB/M process promotes the development of lower thermal gradients and, consequently, slower cooling rates. These conditions enhance the homogeneity of the microstructure across the entire deposited block. This is evidenced by the formation of similar solidified phases in various regions, characterized by coarser Widmanstätten structures and α-lamellae in both the upper and lower areas of the substrate-heated specimens, in contrast to the as-deposited specimens (see Figure 4e,f). An additional stress-relief step applied to the substrate-heated block results in the formation of significantly coarser α-plates, with an average α-lamellae width of ≈4 μm in both the upper and lower regions (see Figure 4g,h).

A unique phenomenon promoted by continuous substrate heating is the nucleation and stabilization of equiaxed grains throughout the entire blocks under both as-substrate-heated and as-substrate-heated-SR conditions (see Figure 3c,d and Figure 5c,d). N. Derimow et al. reported that a HIP process at a high temperature of 1050 °C, applied to additively manufactured specimens produced by the PBF-LB/M process, resulted in an equiaxed prior-β grain morphology.[45] In the present study, the substrate heating temperature is 600 °C, which is below the β-transus temperature. However, the formation of equiaxed prior-β grains is attributed to multiple factors: continuous substrate heating, the high applied laser power, low thermal gradients, and repeated thermal cycling. As a result, the temperature of the molten layers consistently exceeded 1000 °C. These conditions allow the molten layers to remain in the high-temperature β phase field for an extended period, which promotes equiaxed recrystallization of the fully β microstructure. Another effect that enhances the stabilization of equiaxed grain growth throughout the entire block is the combination of a low thermal gradient and high solute segregation. The low thermal gradients result from continuous substrate heating, while the increased oxygen content in the substrate-heated condition acts as a solute element. J. Wainwright et al. reported that the transition from columnar grains to refined prior-β grains in additively manufactured specimens produced by the wire-arc DED process can be achieved by controlling the specific energy density of the deposited material, thereby reducing the thermal gradient.[46] Wang et al. reported that by forcing the feedstock to penetrate the melt pool, they achieved 80 vol% equiaxed prior-β grains in specimens fabricated via the wire-arc DED process.[47] They assumed that a localized negative thermal gradient caused by the feedstock acts as a nucleation front at the top of the melt pool, with additional agitation promoting nucleation and dendrite fragmentation.[47] Applying a high preheating substrate temperature during the PBF-LB/M process promotes the full decomposition of the α′ martensitic microstructure into a stable α + β equilibrium microstructure.[48]

However, the stabilization of equiaxed grains was not successfully achieved by using high preheating substrate temperatures during the PBF-LB/M process.[48] Quasiequiaxed microstructures in PBF-LB/M-manufactured Ti-6Al-4V specimens can be obtained through rapid heat treatment.[49–51]

For both the as-substrate-heated and as-substrate-heated-SR conditions, the same microstructural evolution can be described as follows:

$$(\text{as-substrate-heated/SR})\,\alpha' \rightarrow \beta \rightarrow (\text{coarse})\,\alpha + \beta + \alpha_{GB} \quad (5)$$

The stress relieving treatment and substrate heating result in additional effect compared to the as-deposition specimens. As shown in Figure 7, a continuous increase in oxygen content can be observed relative to both the initial state of the wire and the as-deposition condition. The increase in oxygen content in the substrate-heated-SR specimens reached up to four times higher than in the as-deposited-bulk condition. This rise is primarily attributed to repeated thermal cycling, which introduces additional oxygen into the molten layers. Similar behavior regarding oxygen uptake in additively manufactured Ti-6Al-4V specimens produced by a powder-based DED process was reported by B. E. Carroll et al.[35]

Layered banding (or banded microstructure) typically occurs in additively manufactured Ti-6Al-4V due to cyclic thermal histories during layer-by-layer deposition. These bands often correspond to isothermal lines near critical transformation temperatures (e.g., α-dissolution or the β-transus). In as-deposited specimens, a high thermal gradient dominates, characterized by a steep temperature difference between the melt pool and the surrounding material, combined with short interlayer times. Consequently, heat does not penetrate deeply into the previously deposited layers, minimizing thermal cycling near the β-transus, an essential condition for band formation. As a result, the distinct α-plate coarsening that normally produces bands is suppressed. This has been proved by the solidified fine microstructure in both as-deposited conditions, as shown in Figure 4a–d. In contrast, in substrate-heated specimens, the lower thermal gradient stabilizes the deposited layers at elevated temperatures near the β-transus. This promotes α-dissolution and reprecipitation cycles, thereby enhancing layered band formation (see Figure 3c,d). This phenomenon could be attributed to the development of equiaxed β grains.

4.2. Influence of the Microstructure on the Mechanical Performance

A continuous increase in hardness is achieved by applying stress relief and substrate heating, rising from 336 HV1 for the as-deposited bulk to 436 HV1 for the stress-relieved and substrate-heated condition (see Figure 8a). The formation of fine acicular α′-martensite was observed only in localized and small regions near the substrate under the as-deposited-bulk and as-deposited stress-relieved (SR) conditions; therefore, its effect can be considered negligible (see Figure 5a–d). The stabilization of a more uniform interlocked basket-weave structure and α-lamellae after stress relief and substrate heating is considered the major factor contributing to the increased hardness. A similar behavior was reported by Y. Chen et al. for laser-arc additively manufactured Ti-6Al-4V specimens.[52]

The lowest tensile strength at room temperature was observed in the as-deposited-bulk specimens, with an elongation of ≈6%. After stress relief, an enhancement in tensile strength (850 MPa) and a doubling of elongation were achieved. Both the as-substrate-heated and as-substrate-heated-SR conditions promoted the highest tensile strength of around 1000 MPa, although with a low elongation of ≈3% (see Figure 8b–c). The major microstructural evolution factors during stress relief and substrate heating include the coarsening of the fine Widmanstätten structure present in the as-deposited-bulk condition, leading to the stabilization of coarsened α-lamellar and α-colony structures after substrate heating.

The main factors play a major role in enhancing the tensile properties of Ti-6Al-4V specimens: α-lamella width, α-colony size, prior-β grain size, and prior-β grain boundaries (α_{GB}). Typically, tensile strength decreases with increasing α-lamella width.[44,53] However, this relationship is more complex and should be considered alongside the volume fraction of α-lamellae.[44,53] The tensile strength tends to increase with a higher volume fraction of α-lamellae, up to a tipping point, beyond which very coarse α-lamellae have a significantly negative impact on tensile strength. **Figure 9** illustrates the relationship between α-lamellae width and tensile strength at room temperature under different deposited material conditions. In this study, tensile strength increases with both α-lamellae width and volume fraction, reaching an optimal point for the as-substrate-heated condition. Further stress relieving of the as-substrate-heated specimens leads to excessive coarsening of the α-lamellae, resulting in a decline in tensile strength. Stress relieving (SR) treatment does not significantly alter prior-β grain size, but it thickens α_{GB} and makes grain boundaries more distinct in EBSD maps (see Figure 3a–d and Figure 5a–b). These changes enhance both hardness and tensile strength of as-deposited specimens. However, the β grain size plays a more significant role in influencing the tensile properties of the Ti-6Al-4V alloy than the α-lamellae width. Tensile strength increases as the β grain size decreases. This explains the highest tensile strength observed in the as-substrate-heated condition, which exhibits equiaxed grains, compared to the as-deposited condition that features large columnar grains (see Figure 5a–d). In this study,

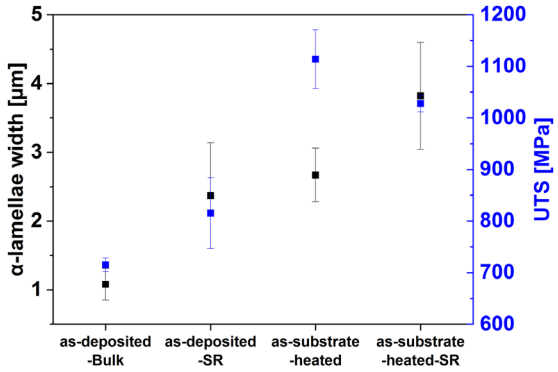

Figure 9. Relationship between α-lamellae width and tensile strength under different deposited material conditions.

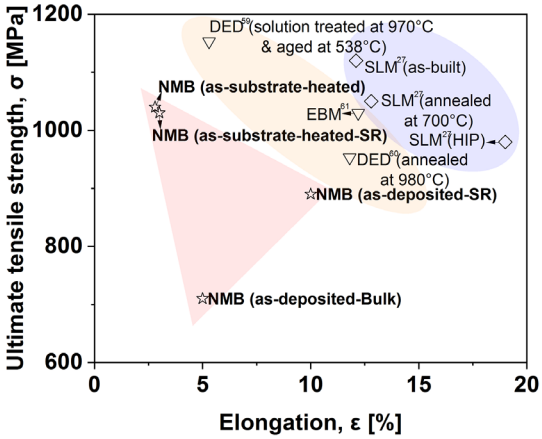

Figure 10. Comparison of the tensile properties of Ti-6Al-4V specimens manufactured using different AM processes at room temperature.

elongation exhibits a decreasing trend with increasing α-lamellae width. This can be attributed to the fact that thick α-lamellae effectively hinder dislocation movement, which reduces the elongation of the as-substrate-heated specimens. An increased oxygen content under as-substrate-heated conditions could be an additional contributing factor to enhanced tensile strength and reduced elongation. B. E. Carroll et al. reported similar positive effects of oxygen uptake, around 125 ppm, on mechanical performance.[35] In this study, the oxygen content under as-substrate-heated conditions is higher, ≈200 ppm.

At 700 °C, the as-substrate-heated condition exhibits the highest tensile strength of 600 MPa, along with the highest elongation of 14%–15%. In contrast, the lowest tensile strength and smallest elongation are observed in the as-deposited-SR condition. This concludes that the refinement of the prior-β grain structure, combined with slower cooling rates resulting from lower thermal gradients, promotes more uniform microstructures, generally more favorable for mechanical performance. B. Meier et al. reported elevated tensile properties of additively manufactured PBF-LB/M Ti-6Al-4V specimens at 500 °C, where the tensile strength under different heat treatment conditions ranged between 660 and 756 MPa, with elongation values of 12%–17%.[54] The elevated mechanical properties obtained at 700 °C in this study, attributed to the full refinement of the prior-β grain structure in specimens manufactured using wire-laser DED, are comparable to those of specimens produced via PBF-LB/M, which were tested at a lower temperature of 500 °C.

The tensile properties of Ti-6Al-4V alloy produced using different AM processes at room temperature are well investigated. **Figure 10** shows a comparison of the tensile properties of Ti-6Al-4V specimens manufactured using various AM processes at room temperature. **Table 4** summarizes the microstructure associated with different AM processes. The highest tensile strength and elongation were achieved by stabilizing a fine α′ martensitic structure using the PBF-LB/M process, followed by optimized two-step heat treatments such as high-temperature annealing combined with ageing at temperatures below 600 °C (the decomposition temperature of α′). Ti-6Al-4V specimens manufactured using the powder-based DED-LB/M process also exhibited a similar range of tensile strength but lower elongation, due to the formation of a fine Widmanstätten structure.[55–57]

The PBF-EB/M process stabilizes a mixed microstructure consisting of fine Widmanstätten, primarily α-phase, and a small amount of β-phase. This results in slightly reduced tensile strength compared to specimens manufactured using PBF-LB/M and powder-based DED-LB/M process. A similar microstructural evolution is observed in the as-substrate-heated specimens examined in this study, which exhibit slightly higher tensile strength. However, the elevated tensile properties at 700 °C for the as-substrate-heated condition are comparable to the tensile properties of Ti-6Al-4V specimens manufactured using PBF-LB/M, which were tested at a lower temperature of 500 °C.

5. Conclusion

Ti-6Al-4V specimens deposited using wire-based DED, followed by stress relieving (SR) and substrate heating at room and elevated temperatures, were investigated.

The as-deposited-bulk and as-deposited-SR specimens exhibit a heterogeneous microstructure consisting of fine acicular α′-martensite and fine Widmanstätten structures within large prior-β grains, with lengths exceeding 10 mm and widths ranging from 1 to 3 mm. Small regions near the substrate show the growth of equiaxed grains.

A full refinement of the prior-β grains was achieved in the as-substrate-heated conditions, with grain sizes ranging from 0.5 to 5 mm. Grain growth is continuous across the layer bands. The microstructure in both conditions consists of coarser transformed α + β colonies, lamellar structures, and Widmanstätten patterns. Very coarse α-lamellae are observed, with average α-lamella widths of 2.5 μm in the as-substrate-heated specimens and 4.0 μm in the as-substrate-heated-SR specimens. Oxygen content increased consistently with processing, from 35 ± 0.8 ppm

Table 4. Summarizes the microstructure associated with different AM processes.

Process	Microstructure	Orientation	σ_{UTS} [MPa]	Elongation [%]	Ref.
PBF-LB/M	very fine Acicular α/α′	Long.	1095 (±10)	8.1 (±0.3)	[24]
		Long.	1143 (±6)	11.8 (±0.5)	[22]
PBF-EB/M	Acicular α + β	Long.	833 (±22)	2.7 (±0.4)	[58]
		Long.	970	12 (±1.2)	[59]
Powder DED-LB/M	α + β α Widmanstätten	Long.	1072 (±33)	17 (±4)	[60]
Wire DED-LB/M	α + β	Long.	1027 (±15)	2.9 (±0.06)	This study

in the initial wire to 197 ± 31 ppm in the as-substrate-heated-SR condition.

The Vickers hardness (HV1) showed a continuous increase upon applying stress relieving and subsequent substrate heating, ranging from 336 for the as-deposited-bulk specimen to 436 for the as-substrate-heated-SR specimens.

The as-deposited-bulk specimens exhibited the lowest tensile strength (750 MPa) at room temperature, with elongation values of 5%–6%. Stress relieving (as-deposited-SR) improved both strength (850 MPa) and ductility (10%–11%). The highest tensile strength (≈1000 MPa) was achieved in the as-substrate-heated and as-substrate-heated-SR conditions but with reduced elongation (≈3%). At elevated temperatures (700 °C), the as-substrate-heated condition demonstrated the best balance of mechanical properties, combining a tensile strength of 600 MPa with superior ductility (14%–15%). These results outperform the other tested conditions and are comparable to those of PBF-LB/M-manufactured Ti-6Al-4V specimens tested at a lower temperature of 500 °C.

Acknowledgements

This work was performed under the auspices of the "Zentrales Innovationsprogramm Mittelstand (ZIM)", under Contract No. ZF4064604LP6. The author would like to thank all colleagues and project partners for their support.

Open access funding enabled and organized by Projekt DEAL.

Conflict of Interest

The authors declare no conflict of interest.

Data Availability Statement

The data that support the findings of this study are openly available in AEM at https://doi.org/10.2708/AEM.1234567, reference number 4412367.

Keywords

DED-LB/M, mechanical properties, prior-β grain, refinement, titanium alloys, vacuum additive manufacturing

Received: August 27, 2025
Revised: October 8, 2025
Published online: November 11, 2025

[1] P. Heinl, L. Mueller, C. Koerner, R. F. Singer, F. A. Mueller, *Acta Biomater.* **2008**, *4*, 1536.
[2] T. DebRoy, H. Wei, J. Zuback, T. Mukherjee, J. W. Elmer, J. O. Milewski, A. M. Beese, A. Wilson-Heid, A. De, W. Zhang, *Prog. Mater. Sci.* **2018**, *92*, 112.
[3] T. Zhang, C. T. Liu, *Materials* **2022**, *1*, 100014.
[4] M. H. Mosallanejad, A. Abdi, F. Karpasand, N. Nassiri, L. Iuliano, A. Saboor, *Adv. Eng. Mater.* **2023**, *25*, 2301122.
[5] T. D. Ngo, A. Kashani, G. Imbalzano, K. T. Q. Nguyen, D. Hui, *Composites Part B* **2018**, *143*, 172.
[6] J. A. Tamayo, M. Riascos, C. A. Vargas, L. M. Baena, *Heliyon* **2021**, *7*, e06892.
[7] A. A. Shapiro, J. P. Borgonia, Q. N. Chen, R. P. Dillon, B. McEnerney, R. Polit-Casillas, L. Soloway, *J. Spacecr. Rockets* **2016**, *null*, 952.
[8] T. Grover, A. Pandey, S. T. Kumari, A. Awasthi, B. Singh, P. Dixit, P. Singhal, K. K. Saxena, *Mater. Today: Proc.* **2020**, *26*, 3071.
[9] M. Koike, K. Martinez, L. Guo, G. Chahine, R. Kovacevic, T. Okabe, *J. Mater. Process. Technol.* **2011**, *211*, 1400.
[10] R. R. Boyer, *Mater. Sci. Eng., A* **1996**, *213*, 103.
[11] A. Hofer, S. Wachter, D. Döhler, A. Laube, B. S. Batalla, Z. Fu, C. Weidlich, T. Struckmann, C. Körner, J. Bachmann, *Electrochim. Acta* **2022**, *417*, 140308.
[12] B. Vrancken, L. Thijs, J.-P. Kruth, J. Van Humbeeck, *Acta Mater.* **2014**, *68*, 150.
[13] T. Vilaro, C. Colin, J. D. Bartout, *Metall. Mater. Trans. A* **2011**, *42*, 3190.
[14] C. Leyens, M. Peters, *Titanium And Titanium Alloys*, Wiley-VCH Verlag GmbH & Co. KGaA, Weinheim, Germany **2003**, pp. 4–7.
[15] D. Eylon, F. H. Froes, R. W. Gardiner, *JOM* **1983**, *35*, 35.
[16] M. J. Bermingham, S. D. McDonald, M. S. Dargusch, D. H. StJohn, *J. Mater. Res.* **2008**, *23*, 97.
[17] A. A. Antonysamy, J. Meyer, P. B. Prangnell, *Mater. Charact.* **2013**, *84*, 153.
[18] D. Zhang, D. Qiu, M. A. Gibson, Y. Zheng, H. L. Fraser, D. H. StJohn, M. A. Easton, *Nature* **2019**, *576*, 91.
[19] I. Yadroitsev, P. Krakhmalev, I. Yadroitsava, *JOM* **2017**, *69*, 2725.
[20] J. Su, F. Jiang, J. Teng, L. Chen, M. Yan, G. Requena, L. C. Zhang, Y. M. Wang, I. V. Okulov, H. Zhu, C. Tan, *Int. J. Extreme Manuf.* **2024**, *6*, 032001.
[21] S. Leuders, M. Thöne, A. Riemer, T. Niendorf, T. Tröster, H. A. Richard, H. J. Maier, *Int. J. Fatigue* **2013**, *48*, 300.
[22] M. Simonelli, Y. Y. Tse, C. Tuck, *Mater. Sci. Eng. A* **2014**, *616*, 1, https://doi.org/10.1016/j.msea.2014.07.086
[23] M. Koike, P. Greer, K. Owen, G. Lilly, L. E. Murr, S. M. Gaytan, E. Martinez, T. Okabe, *Materials* **2011**, *4*, 1776.
[24] Luca Facchini, Emanuele Magalini, Pierfrancesco Robotti, Alberto Molinari, *Rapid Prototyping J.* **2010**, *16*, 450.
[25] Bey Vrancken, Lore Thijs, Jean-Pierre Kruth, Jan Van Humbeeck, *J. Alloys Compd.* **2012**, *541*, 177.
[26] X. Yan, C. Chen, C. Huang, R. Bolot, M. Kuang, W. Ma, C. Coddet, H. Liao, M. Liu, *J. Alloys Compd.* **2018**, *764*, 1056.
[27] G. Kasperovich, J. Hausmann, *J. Mater. Process. Technol.* **2015**, *220*, 202.
[28] B. Zhou, J. Zhou, H. Li, F. Lin, *Mater. Sci. Eng. A* **2018**, *724*, 1, https://doi.org/10.1016/j.msea.2018.03.021.
[29] H. K. Rafi, N. V. Karthik, H. Gong, T. L. Starr, B. E. Stucker, *J. Mater. Eng. Perform.* **2013**, *22*, 3872.
[30] Y. Zhai, H. Galarraga, D. A. Lados, *Eng. Fail. Anal.* **2016**, *69*, 3.
[31] S. M. Kelly, S. L. Kampe, *Metall. Mater. Trans. A* **2004**, *35*, 1861.
[32] G. P. Dinda, L. Song, J. Mazumder, *Metall. Mater. Trans. A* **2008**, *39*, 2914.
[33] D. Clark, M. T. Whittaker, M. R. Bache, *Metall. Mater. Trans. B* **2012**, *43*, 388.
[34] R. Cottam, M. Brandt, *Phys. Procedia* **2011**, *12*, 323.
[35] B. E. Carroll, T. A. Palmer, A. M. Beese, *Acta Mater.* **2015**, *87*, 309.
[36] A. P. Nagalingam, M. Shamir, E. Bugra Tureyen, A. R. Charles Sharman, O. Poyraz, E. Yasa, J. Hughes, *Int. J. Adv. Manuf. Technol.* **2025**, *136*, 2035.
[37] T. Özel, H. Shokri, R. Loizeau, *J. Manuf. Mater. Process.* **2023**, *7*, 45.
[38] G. Zhang, N. Li, J. Gao, H. Xiong, H. Yu, H. Yuan, *Addit. Manuf.* **2022**, *49*, 102511.
[39] T. Klein, J. L. Neves, D. Obersteiner, J. Grillitsch, D. Holec, *Mater. Sci. Eng.: A* **2025**, *943*, 148825.
[40] X. He, H. Yi, W. Zhang, Y. Yin, Y. Liu, H. Cao, *J. Alloys Compd.* **2024**, *1005*, 176196.

[41] Z. Lin, K. Song, Z. Zhu, K. Guo, W. Ya, J. Xiao, X. Yu, *Mater. Sci. Eng.: A* **2023**, *887*, 145750.
[42] P. Åkerfeldt, M. L. Antti, R. Pederson, *Mater. Sci. Eng. A* **2016**, *674*, 428.
[43] T. Ahmed, H. J. Rack, *Mater. Sci. Eng. A* **1998**, *243*, 206.
[44] Y. Liu, F. Chen, G. Xu, Y. Cui, H. Chang, *Metals* **2020**, *10*, 854.
[45] N. Derimow, J. T. Benzing, H. Joress, A. McDannald, P. Lu, F. W. DelRio, N. Moser, M. J. Connolly, A. I. Saville, O. L. Kafka, C. Beamer, R. Fishel, S. Sarker, C. Hadley, N. Hrabe, *Mater. Des.* **2024**, *247*, 113388.
[46] J. Wainwright, S. Williams, J. Ding, *Addit. Manuf.* **2023**, *74*, 103712.
[47] J. Wang, X. Lin, J. Li, A. Xue, F. Liu, W. Huang, E. Liang, *Mater. Sci. Eng.: A* **2020**, *772*, 138703.
[48] H. Ali, L. Ma, H. Ghadbeigi, K. Mumtaz, *Mater. Sci. Eng.: A* **2017**, *695*, 211.
[49] Y. Chong, T. Bhattacharjee, J. Yi, A. Shibata, N. Tsuji, *Scripta Mater.* **2017**, *138*, 66.
[50] Z. Zou, M. Simonelli, J. Katrib, G. Dimitrakis, R. Hague, *Mater. Sci. Eng. A* **2021**, *814*, 141271.
[51] Z. Zou, M. Simonelli, J. Katrib, G. Dimitrakis, R. Hague, *Scripta Mater.* **2020**, *180*, 66.
[52] Y. Chen, J. Fu, L. Zhou, Y. Zhao, G. Feiyun Wang, Y. Qin Chen, *Coatings* **2024**, *14*, 614.
[53] X. Shi, W. Zeng, Y. Sun, Y. Han, Y. Zhao, P. Guo, *Mater. Eng. Perform.* **2015**, *24*, 1754.
[54] B. Meier, F. Warchomicka, J. Petrusa, R. Kaindl, W. Waldhauser, C. Sommitsch, *Berg Huettenmaenn. Monatsh.* **2023**, *168*, 247.
[55] E. Amsterdam, G. A. Kool, *ICAF 2009, Bridging The Gap Between Theory And Operational Practice* (Ed: M.J. Bos), Springer, Dordrecht.
[56] J. Alcisto, A. Enriquez, H. Garcia, S. Hinkson, *J. Mater. Eng. Perform.* **2011**, *20*, 203.
[57] N. Hrabe, T. Quinn, *Mater. Sci. Eng.: A* **2013**, *573*, 271.
[58] P. Edwards, A. O'Conner, M. Ramulu, *J. Manuf. Sci. Eng.* **2013**, *135*, 061016.
[59] E. Brandl, C. Leyens, F. Palm, *IOP Conf. Ser.: Mater. Sci. Eng.* **2009**, *26*, 012004.
[60] J. S. Keist, T. A. Palmer, *Mater. Des.* **2016**, *106*, 482.

